Chapter 3

Development of *in situ* growth method for SWNTs and associated characterization technique

Prior to this PhD work, carbon nanotubes have never been grown at the "Institut für Halbleitertechnik und Nanoelektronik" (in English, "Institute for Semiconductor Technology and Nanoelectronics" or ISTN). However, the increasing interest of the microelectronic community for CNTs, combined with the fact that the ISTN possesses a complete CMOS process line makes the growth of CNTs and their integration into the conventional CMOS technology a possible and exciting challenge. The main aim of this PhD work is the production of nanoelectronic **devices**. Accordingly, a major challenge is the development and optimization of a suitable CNT growth method which allows a CNT integration into a chip. This is the reason why the "*in situ*" growth method for carbon nanotubes has been chosen. "*In situ*" is a Latin expression which means "in the place", so that "*in situ* growth of CNTs" means that the tubes are grown directly in their final place, within the device or circuit on the wafer. The contrary of *in situ* CNT growth is *ex situ* CNT growth, which means that the nanotubes are grown separately, and deposited, after chemical treatment, onto the wafer. Whereas *ex situ* growth of CNTs requires subsequent rearrangement and manipulation of nanotubes, *in situ* CNT growth does not require any reorganization at any step during the device production. This is clearly an advantage for future industrial use where billions of devices have to be produced on a wafer.

Furthermore, this PhD work focuses on the large-scale fabrication of field-effect devices based on carbon nanotubes. The targeted kind of nanotubes are then clearly SWNTs which are the only ones which can be either metallic or semiconducting depending on their chirality. The growth of MWNTs, which are always metallic is then undesirable and should be inhibited. In this chapter, the process developed at the ISTN to grow SNWTs *in situ* as well as the associated parameters are described (section 3.1). Not only the growth process had to be optimized but also a measurement strategy to characterize nanotubes had to be developed, which is presented in this chapter (sections 3.2 and 3.3). Lastly, section 3.4 gives a small summary on the complete growth and characterization method as well as on the results.

3.1 *In situ* growth of SWNTs by means of catalytic chemical vapor deposition (CCVD)

3.1.1 Setup description

CVD furnace for CNT growth

The only known way to obtain SWNTs directly in their final place on a wafer is by means of catalytic chemical vapor deposition (CCVD) of hydrocarbon at high-temperature (600°C-1200°C). Different kinds of furnaces can be used. Most of the furnaces cited in literature are tubular reactors ([10, 70, 71, 72, 73, 74]). For this work, it has been decided to use a bell-shaped reactor with an opaque quartz chamber working at atmospheric pressure. The equipment has been utilized in the past at ISTN for Si_3N_4 CVD (see Fig. 3.1). The volume of the reaction chamber is approximately 30 liters. The wafers lie on a graphite plate coated with silicon carbide which is rotated by a magnetically coupled drive mechanism. The graphite plate is heated via radio frequency induction, working as follows. A copper coil is located under the plate. A high frequency alternating current (200 kHz) passes through the coil so that it produces a magnetic field, which in turn produced a so-called eddy current (also known as Foucault current) in the graphite plate because graphite is a conductive material. These currents lead to a Joule heating of the plate. An optical pyrometer which senses black body radiations of the plate is used to

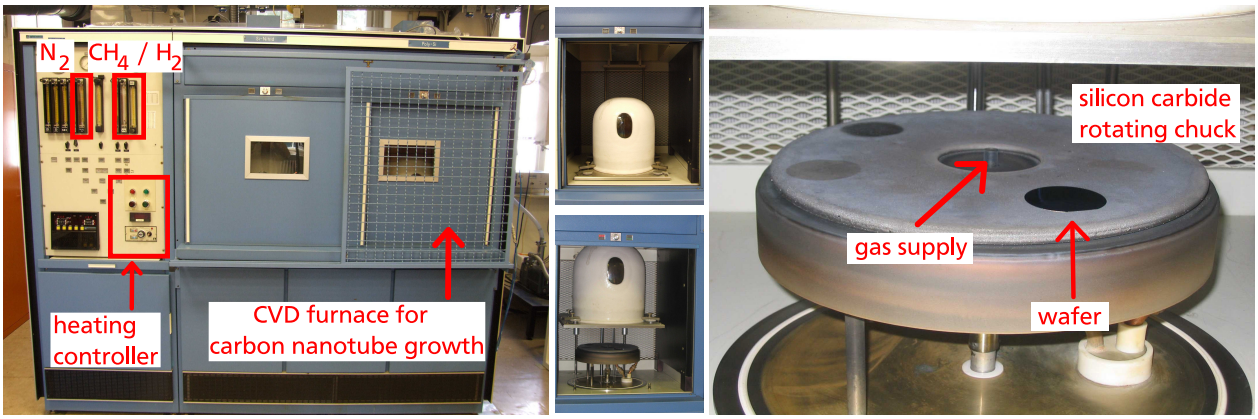

Figure 3.1: Photograph of CVD setup at ISTN. Left: complete setup, middle: reaction chamber (top: closed, bottom: open), right: wafer chuck.

measure the temperature through a transparent quartz glass window. However, the temperature must be adjusted because of non-unity emissivity of the plate and absorption in the quartz wall and glass. Both effects cause the effective temperature to be higher than the one indicated by the pyrometer. The adjustment was done in the past prior to the start of this PhD work. The gases flow through a tube situated at the center of the plate and the exhaust gases flow around the perimeter of the plate. This bell-shaped reactor setup is a novelty for CNT growth because it is the first time this setup is used to grow *in situ* carbon nanotubes for nanoelectronic devices.

Electron beam evaporation equipment for catalyst deposition

The choice of the catalyst which is needed to stimulate CNT growth is an important topic. Frequently, the catalyst is composed of a double layer of metal: an underlayer like aluminum and a catalytic metal like nickel, iron, molybdenum or cobalt. This catalytic metal should exist as nanosized clusters to provide CNT growth. During high temperature growth, the hydrocarbon molecules split into carbon and hydrogen on the cluster surface. Nanotubes then start to be formed by the carbon atoms. The confirmation that such CNTs grow from catalytic clusters was first verified by SEM (see Fig. 3.2) and later on by AFM (see Fig. 3.10 in next section).

Not only CNTs but also metallic clusters can be prepared either *ex situ* or *in situ*. In the *ex situ* case, the clusters are mixed in a solvent and then deposited on the wafer (e.g. by spin coating). *In situ* formation of nanosized clusters occurs when a complete layer of metal is first evaporated on the wafer, and subsequently annealed at high temperature [75]. The high-temperature process step occurs immediately before growth and in inert gas. It has been decided to use a catalyst in form of layer and not *ex situ* fabricated clusters for the sake of simplicity and in view of an industrial integration. In this case, only a standard evaporation setup is needed and the evaporation of a metal layer is a well-known step in CMOS technology in contrast to *ex situ* methods like the separated fabrication, treatment and coating of metal clusters. Moreover, it is much faster than an *ex situ* preparation [75]. However, the setup must provide ultra thin metal layers in the nanometer and sub-nanometer range. We call this form of growth “complete *in situ* growth”, since not only CNTs but also clusters are grown *in situ*.

At ISTN, the deposition of the metallic catalyst is performed by means of electron beam evaporation equipment (Balzer, BPU 100, see Fig. 3.3 top left) the principle of which can be described as follows: The metal is heated until the vapor pressure is sufficiently high to allow its evapo-

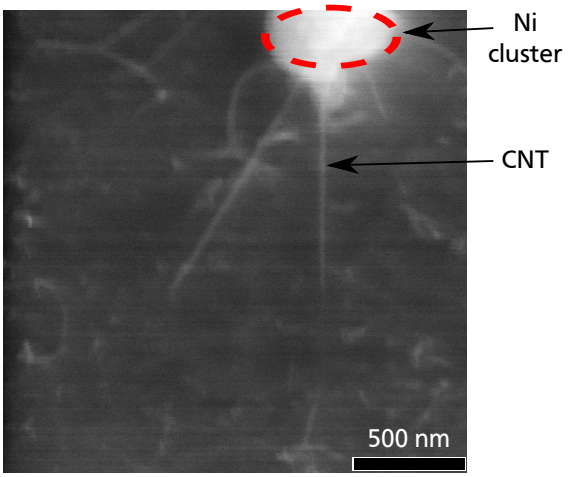

Figure 3.2: SEM micrograph of CNTs grown from cluster. Magnification 50,000.

ration [76]. For this, electrons coming from a filament are accelerated by a high voltage and deflected by a magnetic field towards the metal crucible (see Fig. 3.3 right). When they reach the metal crucible, they are strongly decelerated, which causes heating of the metal which finally evaporates. Moreover, the reaction chamber has been first evacuated untill it reaches an ultra high vacuum (10^{-7} Torr) so that the ablated atoms reach the wafer straightforward without significant scattering with residual gas molecules.

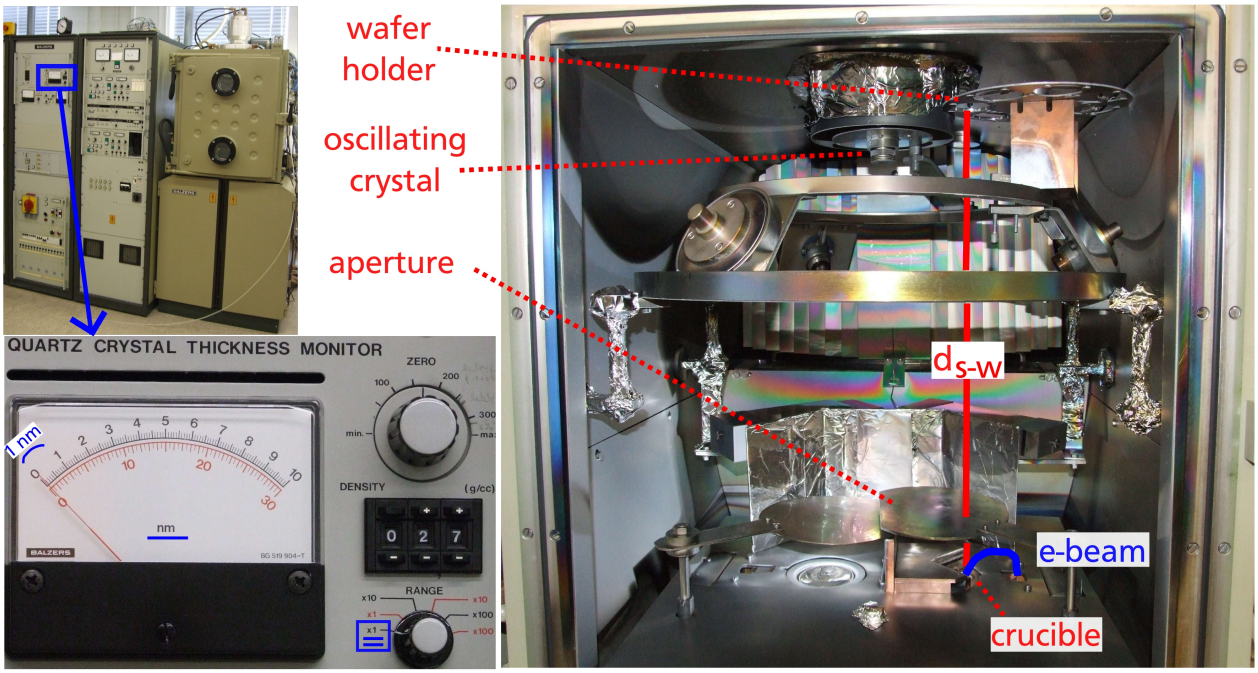

Figure 3.3: Photograph of electron beam evaporation setup at ISTN.

To measure the thickness of the metal film which covers the wafer, an oscillating quartz crystal is embedded in the top of the reaction chamber (see Fig. 3.3 right). It allows a non-destructive and uninterrupted measurement of the thickness of the deposited layer during the evaporation. The thickness is calculated from the shift in the resonance frequency of the crystal. When a metal is evaporated in the reaction chamber, it is continuously deposited on the oscillating

quartz crystal so that the mass of the crystal increases, which decreases its resonance frequency, as summarized in equation (3.1) where f is the quartz eigenfrequency, Δf the frequency shift after evaporation, m_q the primary mass of the quartz and Δm_q the change in its mass caused by the evaporation, i.e., the mass of the deposited layer [77].

$$\frac{\Delta f}{f} = -\frac{\Delta m_q}{m_q} \tag{3.1}$$

If ρ_q is the density of the quartz, d_q its thickness and F its surface, its mass m is equal to $F.\rho_q.d_q$. Similarly, if ρ_l is the density of the deposited layer and d_l its thickness, the mass of the deposited layer Δm is equal to $F.\rho_l.d_l$ for small values of d_l. Replacing these relations in equation (3.1) will lead to equation (3.2) [77] where $K_1 = -\frac{d_q \cdot \rho_q}{f}$ is a specific constant of the quartz.

$$d_l = -\frac{d_q \rho_q}{f}\frac{1}{\rho_l}\Delta f = K_1 \frac{1}{\rho_l}\Delta f \tag{3.2}$$

However, the deposited thickness on the quartz and on the wafer are not necessarily identical. Actually the deposited thickness of a material which is evaporated on a surface depends on the distance d_{S-W} between the source (crucible) and the wafer surface (see Fig. 3.3). The deposited material thickness is inversely proportional to the square of the distance between the crucible and the wafer. In the evaporation setup, the crucible and the quartz have fixed positions. If the wafer is closer to the source than the quartz, the thickness on the wafer will increase and deviate from the thickness calculated from equation (3.2). This is the reason why the constant actually entered in the quartz control monitor in the field "density" (see Fig. 3.3 bottom left) is not $\frac{K_1}{\rho_l}$ but $\frac{K_2}{\rho_l}$, where K_2 contains K_1 and a factor which accounts for the distance effect. For each material, in our case Ni and Al, the factor $\frac{K_2}{\rho_l}$ has to be determined experimentally using test wafers. A layer with a nominal thickness is evaporated on this wafer and then the actual thickness is measured by another method (with AFM for example). From these measurements, the factor $\frac{K_2}{\rho_l}$ can be calibrated exactly. By the next evaporation, the system can precisely compute the deposited thickness on the wafer at any time during the evaporation. For this, it has to measure the shift in the frequency of the oscillating crystal. This is not directly calculated by the difference in the absolute frequency of the quartz at the beginning and the end of the evaporation but with the aid of a second oscillator. Its frequency is calibrated to the frequency of the quartz at the beginning (zero compensation, "ZERO" button on the quartz monitor) and is used as the reference. On the monitor, the changes in the frequency of the second oscillator can be followed in real time on an analog display scaled in nm (see Fig. 3.3 bottom left).

3.1.2 Parameters of SWNT growth

The parameters which play an important role in carbon nanotube CCVD growth can be divided into two groups:

1. **the material**, i.e., the substrate, the underlayer and its thickness, the catalyst and its thickness

2. **the process parameters** of CVD itself, i.e., the gas for annealing and for growth, the flow rate, the temperature, the time etc.

All these parameters can influence the kind of carbon nanotubes which are grown (e.g. SWNTs or MWNTs), their length, their density, their chirality and maybe also their alignment on the wafer (i.e., if they all grow parallel orientated or with random orientation). In this subsection, the most important parameters are discussed in detail. Furthermore, first results on parameter optimization to achieve the selective growth of SWNTs are reported. Note that the optimization process of the parameters is iterative. Later process optimization has been done with the aid of the AFM as a characterization method, as described in the next section (3.2). The final parameters used to produce devices on a large scale have been fixed later on and these results are presented in chapter 4.

Material

Prior to the growth of CNTs, the substrate as well as the underlayer and catalyst must be selected. Several combinations of underlayer/catalyst are investigated whereas silicon wafers are always used as substrates. Nickel is chosen as a catalyst because it is a common and cheap material and it does not, in contrast to iron for instance, cause any contamination of the substrate at high-temperature. It can be observed that the stack Ni/Al/SiO_2 is always favorable for CNT growth whereas the stack Ni/Al deposited directly on the silicon substrate cannot catalyze CNT growth at all. Furthermore, when using Ni/Al as a catalyst but replacing SiO_2 with titan, no CNTs could be grown either.

With a thin aluminum underlayer (10 nm) between Ni and SiO_2, many long nanotubes can be grown (see Fig. 3.4a), with typical diameters of around 30 nm and lengths over 5 μm. However, when Ni is used alone as a catalyst, i.e., when no aluminum is deposited between SiO_2 and Ni, the nanotubes are thicker (typical diameters around 60 nm), shorter (maximal length around 1.5 μm) and have a lower density (see Fig. 3.4b).

Comparing the two SEM micrographs in Fig. 3.4a and Fig. 3.4b, it can also be seen that without aluminum, not only are the nanotubes larger in diameter but also the nickel clusters are larger in size. A possible explanation for the favorable cluster formation for SWNT growth with an Al underlayer is that Al is already fluid at 900°C, which is conducive to the reduction of Ni cluster size (see subsection 3.2.2). The thicknesses of Al and Ni, as well as the total thickness of the Ni/Al catalytic system are, of course, crucial parameters. Typical Al thicknesses are between 5 and 10 nm. The Al thickness influences the spatial density of the nanotubes on the wafer as well as their diameter. If there is too much Al, only thick CNTs (diameter around 30 nm) are grown. If there is not enough Al, the growth of CNTs is completely inhibited. The Ni thickness determines the diameter of the tubes and hence whether SWNTs or MWNTs are grown. Fig. 3.4a and Fig. 3.4c demonstrate the difference in the CNT growth between a 1 nm Ni/10 nm Al and a 10 nm Ni/10 nm Al metal stack. It appears as if for 1 nm Ni, only very few nanotubes are grown. However, this is an artifact: with the SEM, it is only possible to see MWNTs, the diameter of which is around several tens of nm. SWNTs, with a diameter typically between 1 and 3 nm, are invisible due to the limited resolution of the SEM. With 10 nm Ni, numerous MWNTs are obtained. In contrast, with 1 nm Ni, the growth of MWNTs is almost completely inhibited. This result is confirmed by AFM measurements, as presented in subsection 3.2.3.

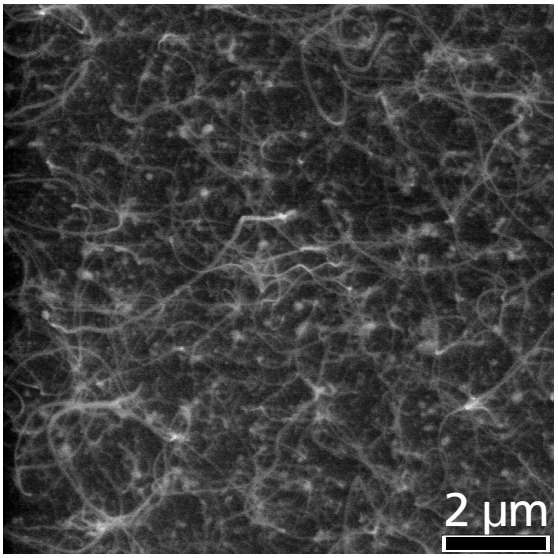

(a) SiO_2: 400 nm; Al: 10 nm; Ni: 10 nm; T: 900°C

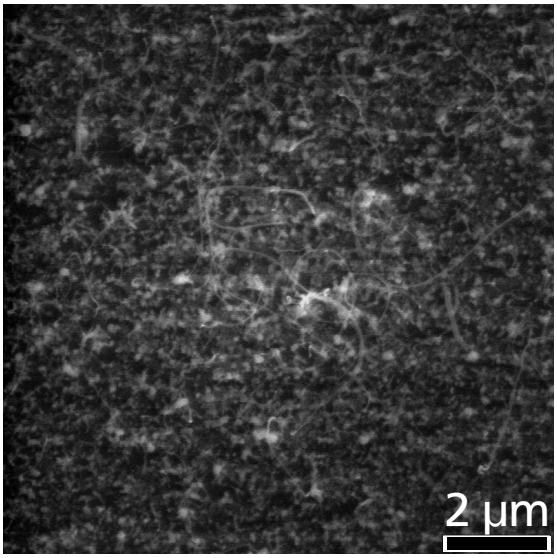

(b) same parameters but without Al underlayer

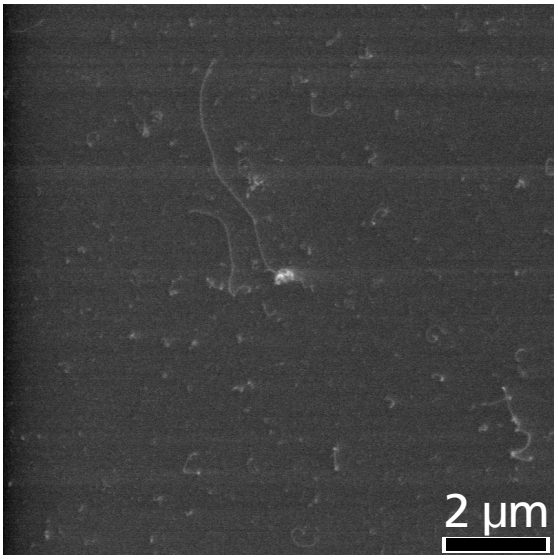

(c) same parameters except for Ni: 1 nm

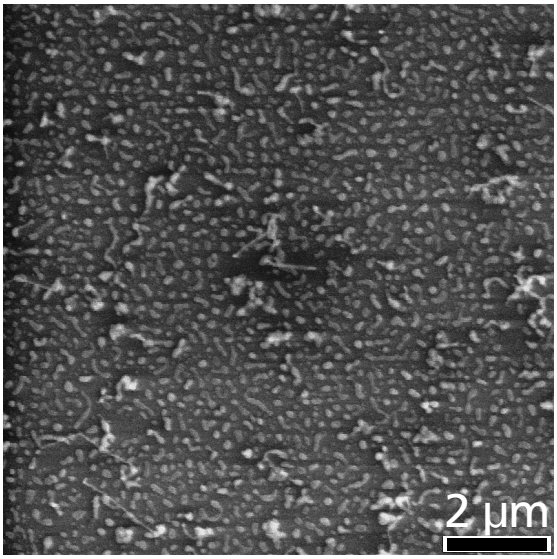

(d) same parameters except for T: 800°C

Figure 3.4: SEM pictures of CNTs grown by CVD. Magnification: 10,000 X.

Growth process parameters

The growth process itself takes place in two steps:

1. Annealing of the wafers in inert gas (typically argon [75] or nitrogen [78]) or in hydrogen [79] to form nickel nanoclusters
2. CVD of CNTs from a hydrocarbon gas

Preliminary experiments are performed to compare H_2 and N_2 as annealing gases. With a non-optimized flow rate, no CNTs at all can be obtained by annealing the wafers in H_2 whereas N_2 provides good results. Even though the growth of CNTs could probably be obtained with an optimized H_2 flow rate, N_2 is chosen as it is cheap (compared for instance with argon) and immediately gives good results. In all the experiments and results presented in this PhD work, the annealing of the wafers before CVD has been performed in N_2 (6 l/min) during 5 min.

For CVD itself, a CH_4 supply has been added to the reaction chamber of the furnace because it is known to be a good feedstock for SWNT CVD growth, as reported for the first time by Kong et al. [33]. Undiluted CH_4 is primarily used, with a flow rate of 6 l/min. In further experiments, CH_4 is diluted with a small quantity of H_2 to inhibit the pyrolysis of CH_4 and to prevent the deposition of an amorphous layer of carbon on the wafer (see section 4.3). Subsequently, the temperature and the duration of CVD need to be determined. Since the temperature of the CVD reactor is measured with an infrared detector, only temperatures above 700°C are reliably measurable. 800°C and 900°C have both been tested as growth temperatures. The results are shown in Fig. 3.4a and Fig. 3.4d. No major differences can be perceived. By using a temperature above 1000°C, the pyrolysis of methane starts to become visible by the black fume in the reactor so that these experiments have to be interrupted for safety reasons. Note that in all experiments reported in this work, the same temperature is used for both annealing and CVD steps. Finally, experiments to optimize the growth time have been performed. 10 min for the growth provides optimal results, however, CNTs start to appear already after 2 min.

3.2 Characterization of *in situ* grown SWNTs by atomic force microscopy (AFM)

In the previous section, SEM micrographs of *in situ* grown CNTs have been presented. However, SWNTs stay invisible on the SEM images because their diameter, of around 1 to 3 nm, is below the SEM resolution. Furthermore, micrographs with a magnification above × 50,000 are blurred. A better characterization method for *in situ* grown CNTs should be found. The atomic force microscope has been selected to investigate the surface of wafers covered with CNTs. The results, as well as a quick introduction to the AFM principle are presented in this section.

3.2.1 Principle of AFM and presentation of AFM Dimension 3100

The original idea of the AFM dates from 1929. In this year, Gustav Schmalz invented the stylus profiler, precursor of the AFM [80]. By AFM, a tip, suspended under a so-called cantilever (see Fig. 3.5 bottom left), moves on the surface of the wafer. A laser beam which is focused on the cone end of the cantilever (see Fig. 3.5 top for a schematic of AFM) is reflected in the direction of a photodetector. The change in the reflection angle which is caused by the surface topography is

measured by the position-sensitive photodetector. Pictures of the surface topography are drawn by the computer by attributing to each different detected angle a color which itself corresponds to a height.

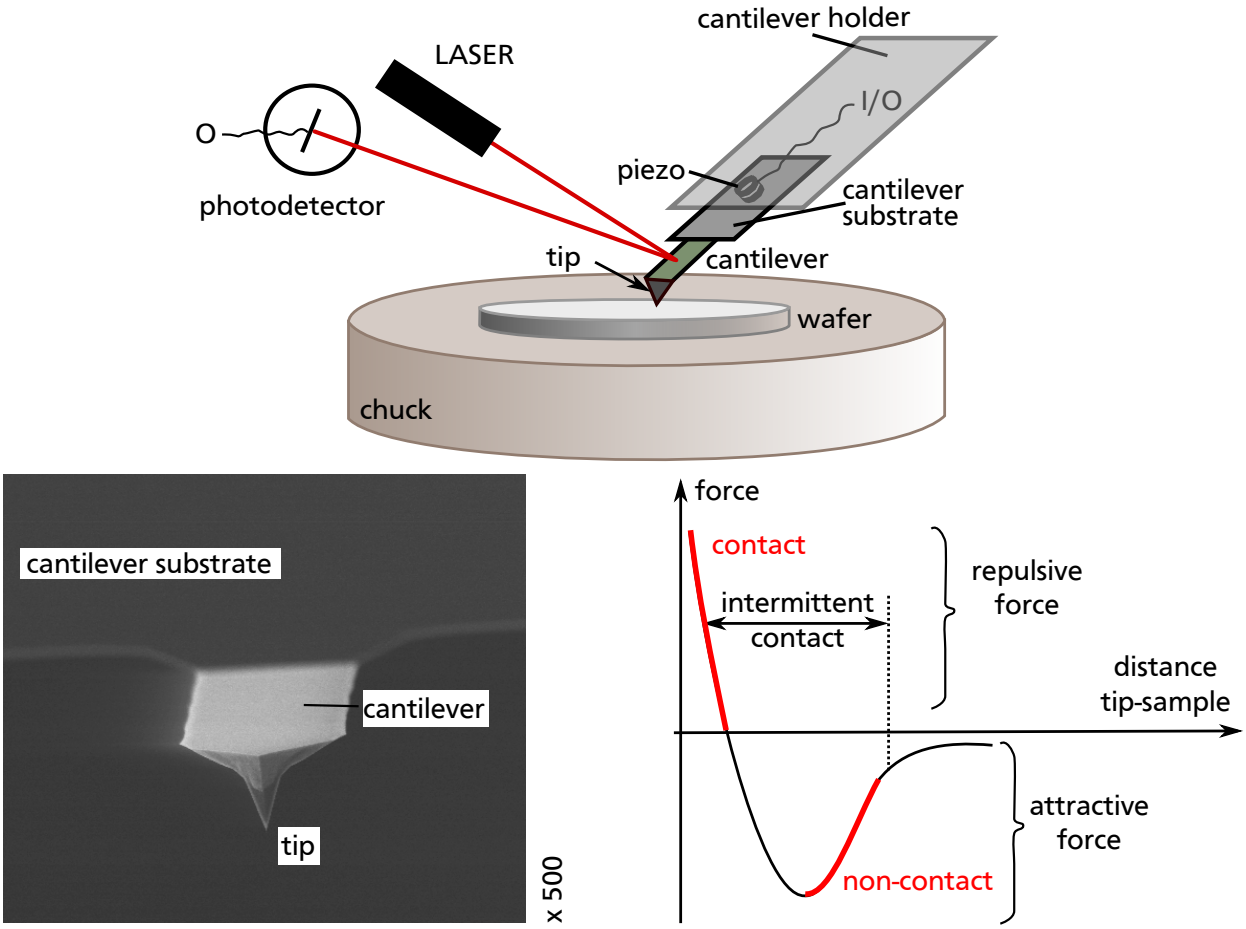

Figure 3.5: Top: schematic of AFM, Bottom left: SEM micrograph of a silicon cantilever (Budget Sensors) substrate, magnification: 500. Bottom right: Interaction force versus distance between tip and sample (the force is the deviation of the Lenard-Jones potential), reproduced from [81].

The field is scanned line after line. To regulate the force applied by the tip on the surface and allow the detection of tiny movements of the cantilever, the vertical position of the cantilever above the sample has to be precisely controlled and measured. For this, piezoelectric materials are used as they elongate/contract when a voltage difference is applied and alternately they generate a voltage difference under compressive/tensile stress. Since the piezoelectric materials are highly sensitive, typical resolutions in the picometer range can be obtained when measuring with AFM.

Three AFM modes exist to detect the topography of the surface: contact-mode, non-contact-mode and tapping-mode (or intermittent contact-mode). These modes differ in the operating distance between sample and tip during the measurement. By AFM, the interactions between tip and sample occur in the atomic range, this is the reason why they can be described by the Lenard-Jones potential, which is composed of attractive interactions (van der Waals interactions) and repulsive interactions (Pauli repulsions). From the Lenard-Jones potential, an interaction force between tip and sample is created, which depends on the tip-sample distance.

This force is plotted in Fig. 3.5 bottom right, as well as the operation distance regions for the three AFM modes.

In the non-contact mode, the cantilever does not touch the sample but stays away from the sample surface and oscillates at or near its natural resonance frequency. The shift from its natural resonance frequency, which is due to sample attractive interactions, is measured by the piezoelectric material.

In the contact mode, the cantilever tip remains in contact with the sample. The forces between tip and sample are repulsive.

The tapping mode combines qualities of both the contact and non-contact modes: the cantilever oscillates at or near its natural resonance frequency, but also impacts the sample surface for a minimal amount of time. The tapping-mode is the most appropriate mode for soft surfaces which should not be damaged. The excitation of the cantilever occurs with a constant energy so that the deflection of the laser beam caused by the oscillation of the tip is also constant. This implies that a change in the deflection corresponds to a change in the surface topography, in the same way as for contact mode AFM.

The AFM at ISTN is a Dimension 3100 from Digital Instruments/Veeco (see Fig. 3.6 right for a photo of the AFM). This setup can perform measurements in contact-mode and tapping-mode. By scanning a field in tapping-mode, two different pictures are obtained. One is the "height" picture, the other is the "amplitude" picture. Both are recorded simultaneously during the scan of the sample. The height picture is computed from the output signal measured at the piezoelectric material (see Fig. 3.5 top). The signal (voltage difference) is proportional to the changes in the piezoelectric material height. The height picture represents the topography of the surface: cross sections can be carried out to obtain a profile of the structure, step heights can be measured. However, this picture does not present a clear overview of the surface because the edges look rounded. For the amplitude picture, the output signal of the photodetector, which records the changes in the reflection angle of the laser (caused by the vertical moves of the cantilever) is used. The amplitude picture provides, in contrast to the height picture, a sensitive edge detection technique so that significant overviews of surfaces are obtained. However, this picture cannot be used for cross sections and step height measurements.

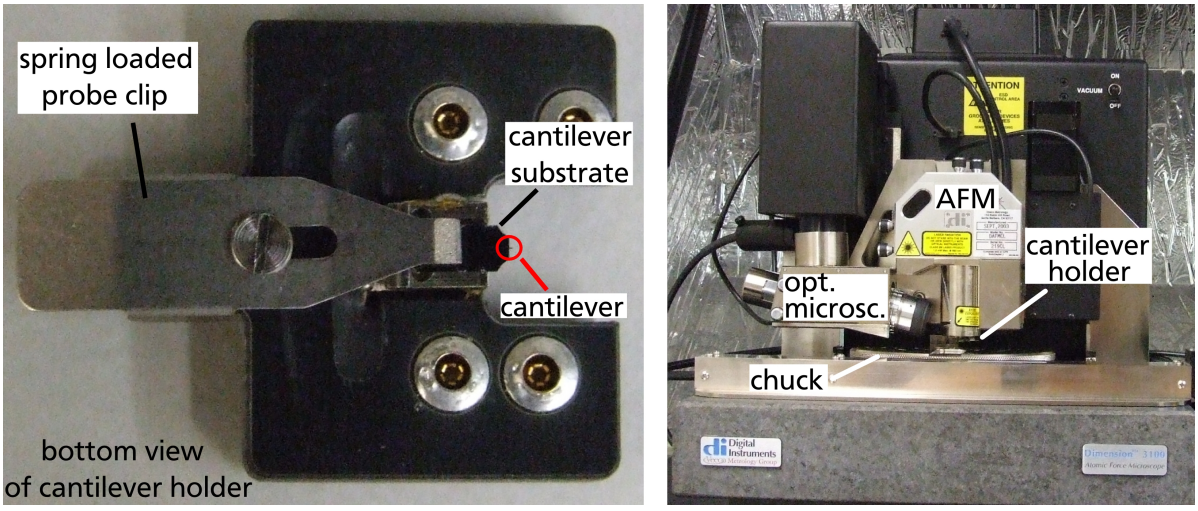

Figure 3.6: Left: bottom view of cantilever holder from AFM Dimension 3100. Right: Photo of AFM Dimension 3100 (Digital Instruments/Veeco).

The procedure for measuring wafer surface with AFM is as follows: The sample is placed on the chuck and held by vacuum. The cantilever substrate is mounted on the cantilever holder (see Fig 3.6 left), which is located under the AFM module (see Fig 3.6 right). Then, the laser beam has to be aligned on the top of the cantilever, the photodetector has to be adjusted so that the deflected laser beam points into the middle of it. The embedded optical microscope which is used to focus on cantilever and sample has to be set first on the end of the cantilever and then on the targeted place on the sample. The resonance frequency of the cantilever is calculated automatically by the system. Lastly, the tip is driven to contact to the surface and the measurement can begin. Prior to the measurement, several parameters have to be adjusted, e.g. the scan size, the length/width ratio, the velocity of the tip. During the measurement, other parameters must be set to obtain a good scan: the amplitude setpoint and the integral and proportional gains. The amplitude setpoint influences the force which is applied by the tip on the wafer surface. The integral and proportional gains must be sufficiently high to force the system to follow the topography of sample surface. If they are too low and the structures to be scanned tall, tip and sample can be damaged because the amplitude of the cantilever oscillations is too small. However, if the gains are too high, the tip will be excessively far away from the surface and the resulting scan will show parasitic oscillations. The three parameters have to be set very precisely to obtain an accurate scan of the structure without damaging it. During each measurement, three pictures with different parameters (height or amplitude pictures, different scaling) can be produced simultaneously. If the integral and proportional gains are sufficiently high, the amplitude picture represents the derivative of the height picture. [82]

3.2.2 Basic AFM measurements on catalyst and SWNTs

Numerous investigations on CNTs can be performed with AFM, however, preferably in tapping-mode because of its superior resolution combined with low tip-sample interaction. With the contact mode, thin SWNTs cannot be resolved. All scans presented in this section (3.2) are realized with tapping-mode AFM, called only “AFM” to simplify matters. The two pictures obtained during an AFM scan in tapping-mode, i.e., height and amplitude pictures (see subsection 3.2.1), are called in this section and everywhere else in this dissertation “AFM scan (height)” and “AFM scan (amplitude)”.

CNT and catalyst measurements after processing

A first result of AFM measurement (height scan) on *in situ* grown carbon nanotubes is given in Fig. 3.7. In the color scan, some nanotubes can be easily recognized as well as clusters. However, from the cross section, it is not possible to identify the different materials which lie on the surface because of excessive topography: nanotubes and clusters are very close to each other as well as tangled. Accordingly, using AFM directly on the catalyst to detect CNTs is not so easy due to increased surface roughness. To avoid these problems, the catalyst (i.e., Al/Ni) is structured on SiO_2 before CNT growth. For catalyst patterning, standard lithography and lift-off processes are used to produce catalytic areas with a width of around 5 μm. The length of the catalytic areas is, however, much more elevated (several hundreds of μm) because it is aimed to use subsequently the Al/Ni areas as contacts for SWNTs (see section 4.2). After structuring, the wafers are processed in the CVD reactor in the same way as unstructured wafers. The CNTs

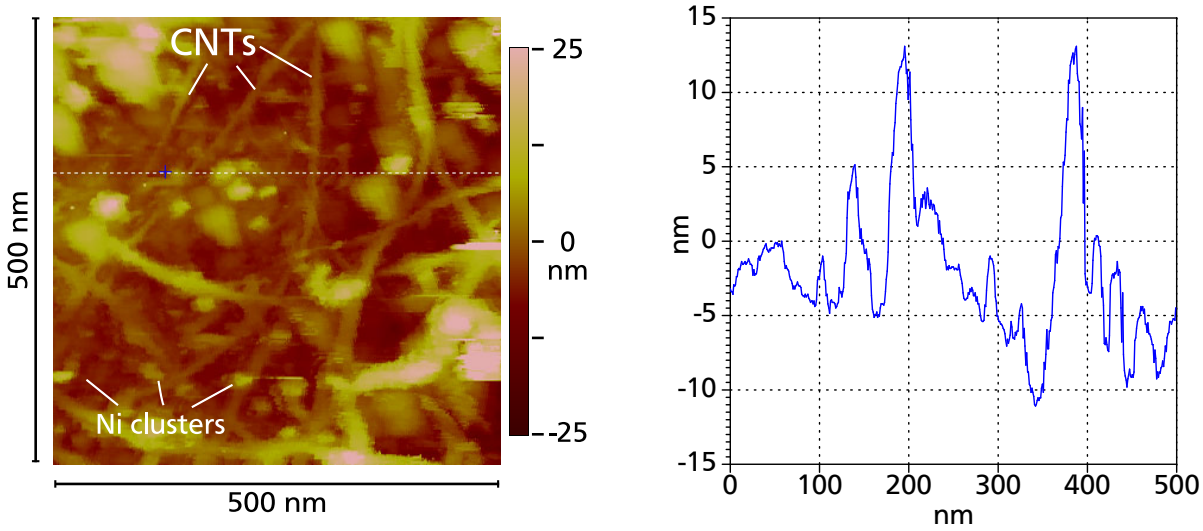

(a) AFM scan (height)

(b) cross section along the white line

Figure 3.7: First example of AFM measurement of CNTs grown *in situ* by CVD on unstructured Al/Ni catalyst

extending from the structured catalyst and lying on the smooth SiO_2 are then characterized by AFM. In fact, the SiO_2 layer which acts as the underlayer for catalyst and nanotubes is found to be very smooth so that even nanometer scaled objects can be detected by AFM (see appendix page 141). An example of an AFM scan on a wafer with a patterned catalyst after processing and CNTs lying on SiO_2 is given in Fig. 3.8.

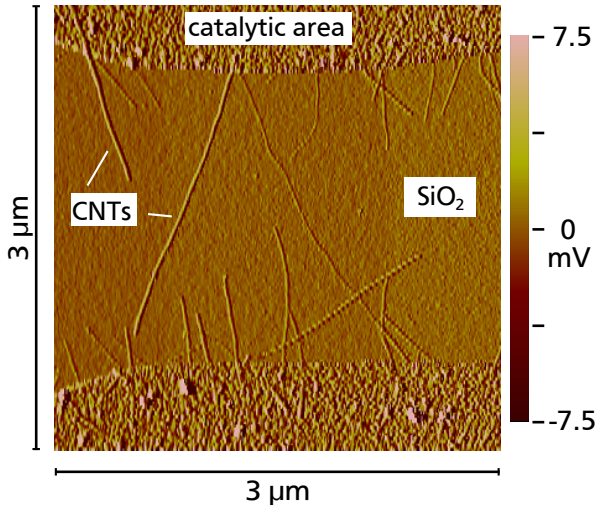

Figure 3.8: Example of AFM scan (amplitude) of CNTs extending from structured catalytic area and lying on smooth SiO_2.

The wafers are also investigated by SEM. Fig. 3.9 left shows an SEM overview of the structured catalyst after processing. The SEM micrograph indicates that some large-diameter MWNTs have grown but stand preferably perpendicular on the metal surface without reaching the oxide. The thinner CNTs lie horizontally on the oxide and partly link adjacent metal stripes. To investigate

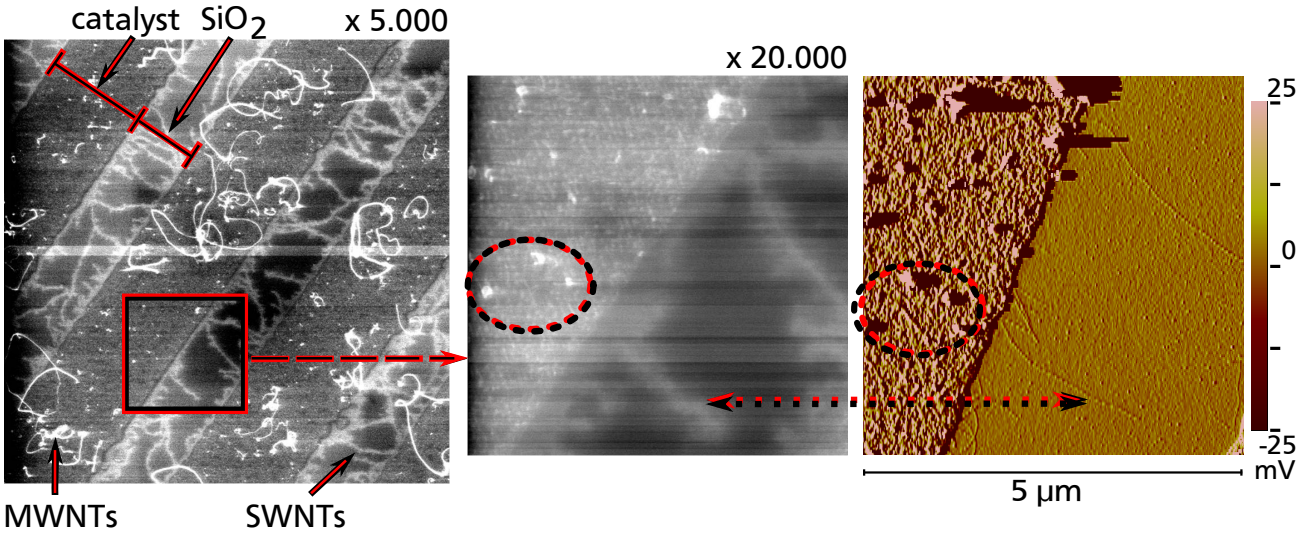

Figure 3.9: Left: SEM overview of structured catalyst on SiO_2. Middle and right: Comparison of SEM micrograph with AFM scan (amplitude) showing exactly the same place on the wafer.

the nature of the thin CNTs, an SEM magnification at the SiO_2/catalyst edge on a location (25 μm^2) free of standing MWNTS as well as an AFM scan showing exactly the identical location with the same scale as the SEM micrograph are recorded. The results are presented in Fig. 3.9 middle and right. This comparison indicates that the thin CNTs lying on the oxide are SWNTs (AFM diameter: 1 - 3 nm), even though their apparent diameter measured by SEM is much larger (20 - 50 nm) than typical SWNT diameters and may suggest MWNTs. The larger size of the SWNTs measured by SEM is due to charging effects causing apparent broadening [83]. Without charging effects, SWNTs would be invisible in the SEM image because their diameter is below the SEM resolution. This also explains why SWNTs are not seen on the metal electrode, since charging effects are absent and thus no broadening is possible.

As explained in subsection 3.2.1, the amplitude picture obtained by an AFM scan gives a very good edge contrast and is the most appropriate AFM measurement for observation of structured surfaces. This is the reason why the amplitude scan has been used for comparison with the SEM

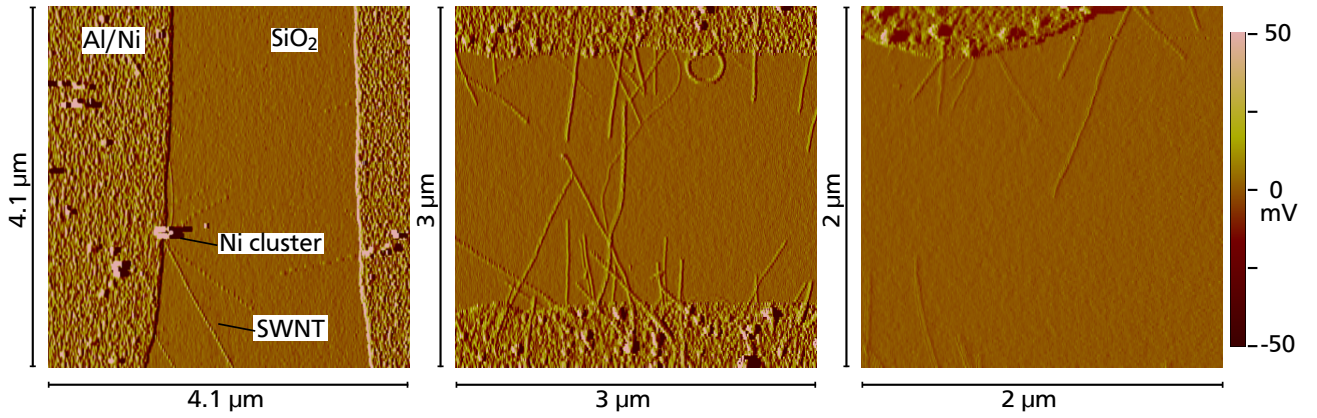

Figure 3.10: Three examples of AFM scans (amplitude) illustrating CNTs growth from Ni-clusters.

measurements (see 3.9 right). Similarly, Fig. 3.10 shows three amplitude scans which clearly

prove that SWNTs grow from Ni-clusters.

Investigation of Al roughness

As already mentioned, aluminum plays a major role in the formation of optimal catalyst clusters, probably due to its low melting point (around 660°C [84]). Without Al, the CNT growth is almost completely inhibited (see Fig. 3.4b). Different explanations can be found in literature to explain the role of Al:

1. Al hinders the formation of large Ni clusters by inhibiting the surface diffusion of Ni atoms. Indeed, on Al, the Ni atoms cannot diffuse as fast as on SiO_2: The surface diffusion rate of an atom depends on the roughness of the underlayer, and Al is rougher than SiO_2 because it has been deposited by electron beam evaporation [71].

2. The low melting temperature of Al helps to improve the nucleation density of the catalyst particles [75].

To confirm these explanations, the roughness of Al is investigated by AFM. The results are shown in Fig. 3.11. The Al layer has been structured on SiO_2 and has a thickness of 10 nm, as confirmed

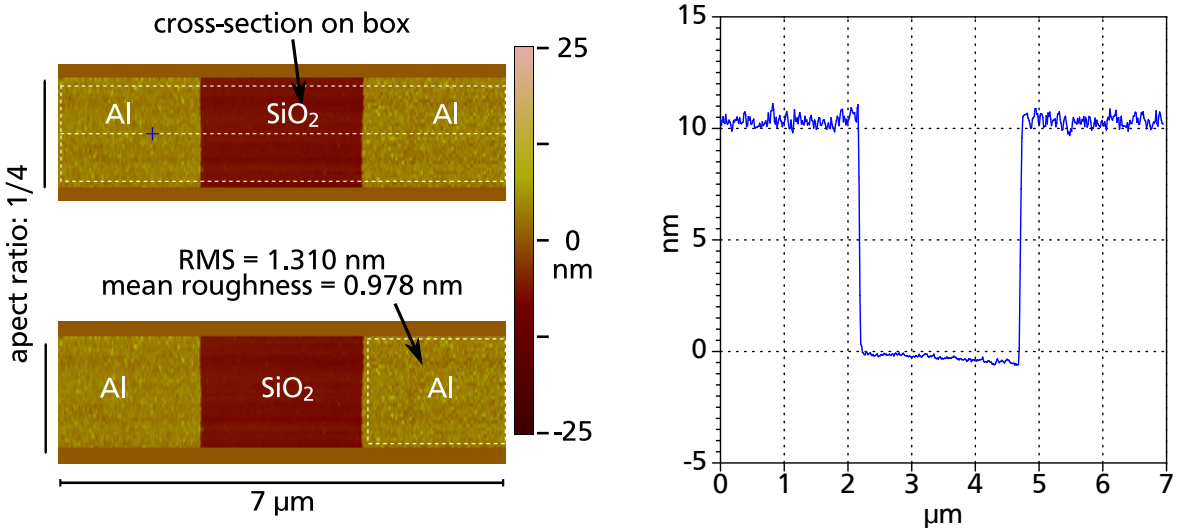

(a) AFM scan (height), represented twice. Top: cross section measurement. Bottom: roughness measurement.

(b) Cross section average of all scanned lines contained in the white box in the top scan.

Figure 3.11: AFM measurement of aluminum structured on SiO_2.

also by AFM (see Fig. 3.11b). The Al roughness is found to be around 1-1.3 nm (RMS-mean roughness), which appears comparable to SiO_2 roughness (0.3-0.4 nm for a 30 nm thick layer, see appendix page 141). However, the relative roughness should be computed to be able to compare both SiO_2 and Al layer:

- **SiO_2:** thickness: 30 nm / roughness: 0.3-0.4 nm ⇒ relative roughness: 1-1.3%
- **Al:** thickness: 10 nm / roughness: 1-1.3 nm ⇒ relative roughness: 10/13%

The ten times more elevated Al roughness combined with the fact that Al smelts at 660° can explain the formation of Ni particles in the nanometer range and hence the successful SWNT growth on Al/Ni stacks.

Oxygen plasma influence

Another possibility to improve SWNT *in situ* growth has been investigated during this PhD: the influence of the oxygen plasma treatment of the catalyst before CVD. A gentle oxygen plasma treatment (low energy, 5 min) was originally used to remove remaining organic rests on the patterned catalyst after lithography. However, the treatment is also found to influence SWNT growth, as confirmed by the following test: A test wafer is split into two parts and the parts are processed simultaneously for all steps except the O_2 plasma. Fig. 3.12 shows the AFM measurements of two equivalent structures, each one on a different part of the wafer. Looking

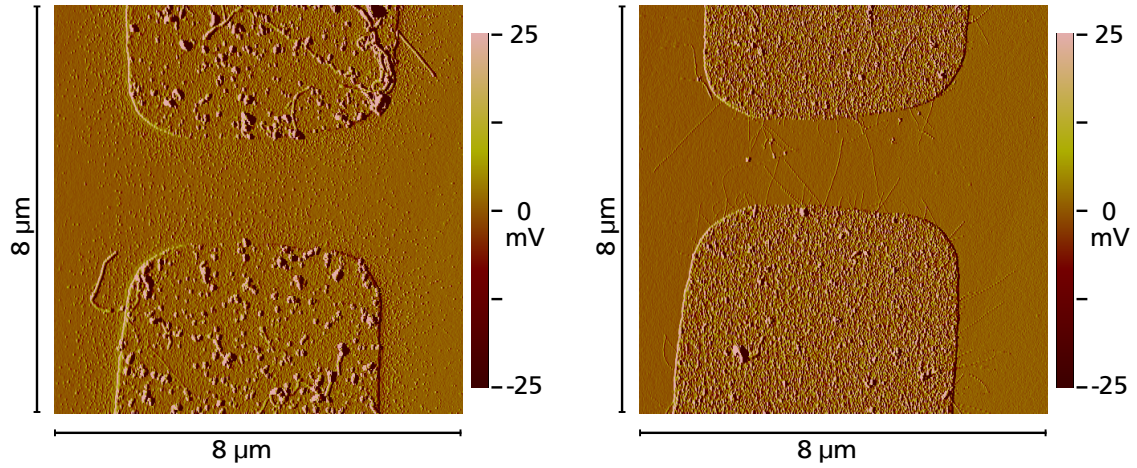

Figure 3.12: AFM scans (amplitude) showing the difference in cluster formation and in density and size of nanotubes without (left) and with (right) oxygen plasma.

at the two AFM amplitude scans, the influence of the O_2 plasma on the nanotube growth is obvious. The nanoclusters are seen to be much smaller and through it, the diameter of the SWNTs is clearly reduced, whereas their density is increased. This supplementary step in the growth process is used in all experiments reported in this work, even when no patterning of the catalyst i.e., no photolithography step occurs before.

3.2.3 AFM optimization of catalyst thickness to control SWNT diameter

In this subsection, the first important optimization step is discussed: the control of the diameter of the *in situ* grown CNTs. It is essential for several reasons. To ensure the selective growth of SWNTs over MWNTs, the CNT diameter must be below 3 nm. Also the diameter of s-SWNTs determines their band gap (see equation (2.16), subsection 2.2.4): the smaller the diameter, the larger the s-SWNT band gap and hence the better the difference between on and off currents of the eventual field-effect transistor in which s-SWNTs serve as channel. For a 3 nm SWNT, E_g is equal to 0,27 eV whereas for a 1 nm SWNT, E_g is equal to 0,8 eV. However, the control of the chirality and thus the metallicity (semiconducting or metallic) of SWNTs is not possible solely

through the selection of the diameter because measurment accuracy needs to be in the low pm range (see subsection 2.2.3, especially Table 2.2 together with Fig. 2.7). In this subsection, AFM methods to measure the diameter of *in situ* grown SWNTs and to aid in the optimization of the catalyst parameters to obtain the selective growth of SWNT over MWNTs are described.

Catalyst thickness measurement

Prior to CNT growth, the catalyst thickness has to be controlled after electron beam deposition. For this, the "stepheight" routine in the old version of the AFM program (Nanoscope 5.12r5) is used. An example of such a measurement is given in Fig. 3.13. The stepheight func-

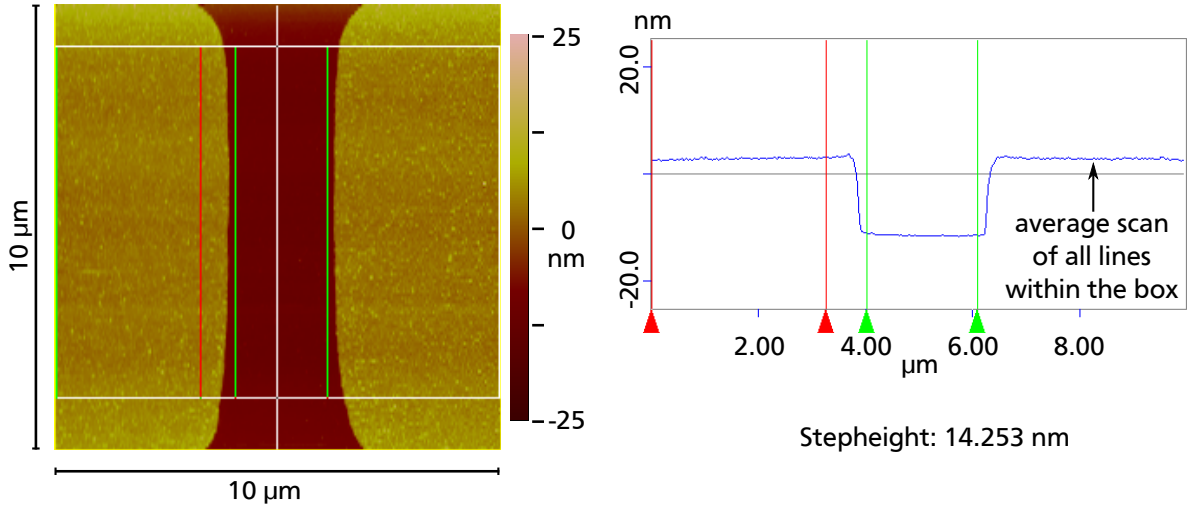

Figure 3.13: Left: AFM scan (height) on evaporated catalyst (Al/Ni, nominal thickness: 15 nm) before growth. Right: associated measurement of stepheight with AFM function "stepheight".

tion computes an "average scan line" over all lines within the selected box. It also indicates the height difference between two segments by computing the average height of each segment and subtracting both average heights. The selected segments are delimitated by the color arrows. This function is unfortunately absent in the newest version of the AFM program (Nanoscope 6.12r1) which is otherwise used in this work. In Fig. 3.13, the measured stepheight (effective thickness of the catalyst stack) is 14.2 nm whereas the nominal thickness given by the quartz monitor of the electron beam deposition setup is 15 nm (5 nm Ni on 10 nm Al). To obtain a reliable statement of the effective thickness, several measurements on different places of the wafer are performed and a mean value computed. The AFM effective thickness of the metal stack is found to sometimes deviate from the quartz nominal thickness. Although the calibration of the crystal quartz is regularly controlled, small remaining deviations between nominal thicknesses and AFM measurements could not be avoided. Moreover, catalyst thickness measurements become impossible when the catalyst is not structured anymore (this is the case in subsequent tests reported in chapter 4) for evident reasons: only layers with steps can be measured by AFM. A direct control via AFM of the thickness on unstructured metal layers is not possible. Two solutions of indirect control have been investigated:

1. Unstructured test wafers are simultaneously evaporated with the unstructured batch wafers. The metal layer of the test wafers is structured after evaporation. However, it appears difficult to etch Ni. With wet etching, the structures are not sufficiently sharp to ensure viable

AFM measurements. With dry etching, the selectivity of Ni/Al over SiO_2 is insufficient to exclude that e.g. a few nm of Al remain on the wafer or some nm of SiO_2 have been etched off together with the metal.

2. Test wafers covered by a structured layer of photoresist are simultaneously evaporated with the unstructured batch wafers. Patterning of the metal layer occurs by lift-off and the metal thickness is measured by AFM. However, the fact that a wafer has structures could influence the thickness of the deposited metal layer due to shadowing effects during the electron beam evaporation, especially when the structures are narrow.

Catalyst thickness optimization and SWNT diameter measurements

To achieve the required selective growth of SWNTs, numerous Al/Ni combinations are investigated. Their influence on the SWNT diameter needs to be determined. At the beginning of this PhD work, a statistic evaluation of CNTs grown on the 10 nm Ni/10 nm Al combination was performed. Fig. 3.14 shows the resulting diameter distribution. The majority of the nanotubes have a diameter between 2 and 4.5 nm. Tubes with diameter over 2.5 nm are most likely constituted of several carbon shells (i.e., MWNTs) for energetic stability reasons. Also, even if the 4 nm CNTs would be single-walled and semiconducting, their corresponding band gap would be excessively reduced (0.2 eV). Accordingly, they cannot act as the channel in field-effect devices because these devices would show a transfer characteristics with a very low on/off ratio. Therefore, this catalyst combination is inappropriate to realize high-performance CNTFETs.

Quartz		AFM	
Al thick. (nm)	Ni thick. (nm)	Step height (nm)	SWNTs diam. (nm)
10	10	17	>3
10	5	14	~ 1.5
10	1	11	~ 1.5
9	1	10	~ 1.2
7	0.9	7	~ 1
5	0.9	6	~ 1

Table 3.1: Comparison of nominal and effective Al/Ni thicknesses, influence on SWNT diameter.

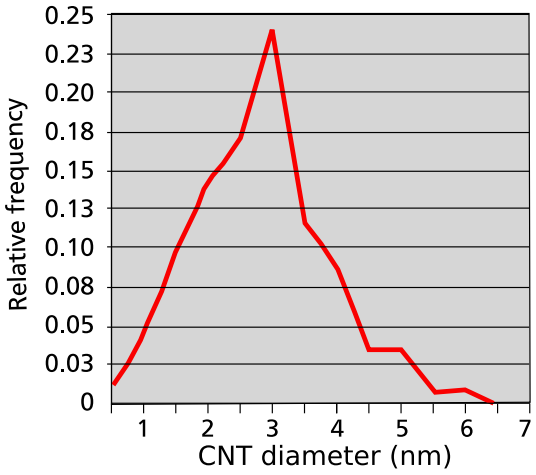

Figure 3.14: Distribution of diameter (measured by AFM) of CNTs grown on 10 nm Ni/10 nm Al.

In order to reduce the SWNT diameter, the influence of the nickel thickness has been studied. 10 nm Al are used in all experiments of this study whereas the nominal Ni thickness is reduced from 10 to 1 nm. The results are shown in Fig. 3.15 and Table 3.1. Looking at the three AFM scans together with the cross sections, it can first be concluded that reducing Ni nominal thickness when keeping constant Al thickness does not seem to influence the number of SWNTs per μm^2. On the other hand, reducing Ni thickness decreases the diameter of nanotubes, but only until a certain limit is reached. When reducing the Ni layer thickness from 10 nm to 5 nm, the SWNT diameter reduces drastically from ~ 3-4 nm to ~ 1 to 2 nm. However, when reducing

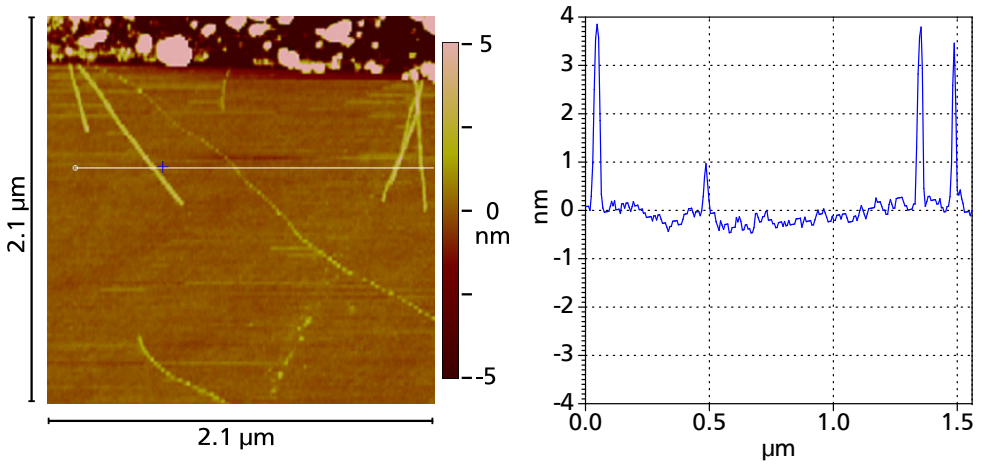

(a) Al: 10 nm, Ni: 10 nm

(b) SWNTs Ø: > 3nm

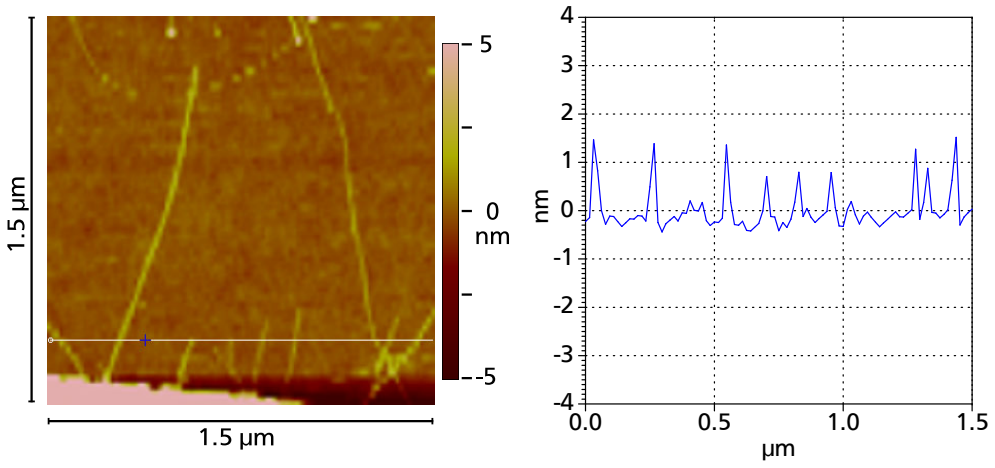

(c) Al: 10 nm, Ni: 5 nm

(d) SWNTs Ø: ∼ 1.5nm

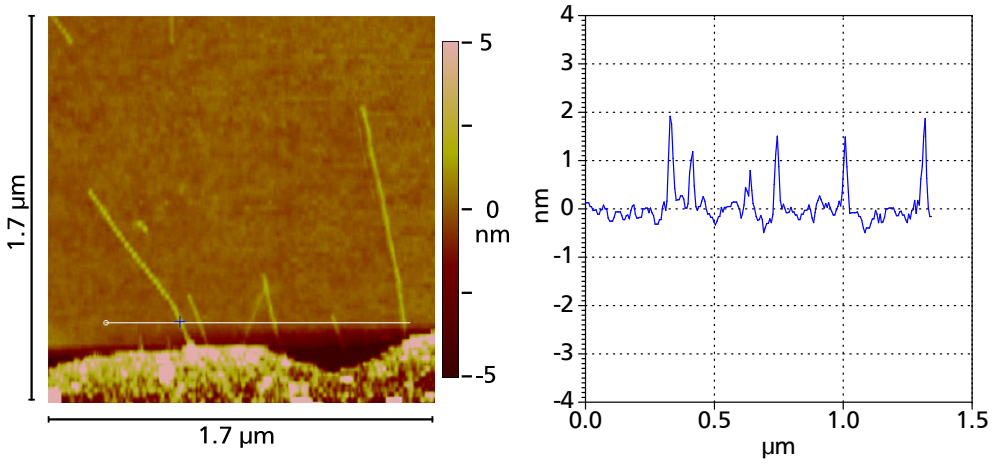

(e) Al: 10 nm, Ni: 1 nm

(f) SWNTs Ø: ∼ 1.5nm

Figure 3.15: Influence of Ni thickness on SWNT diameter for a constant Al nominal thickness (10 nm). Left column: AFM scans (height). Right column: cross sections along respective white lines.

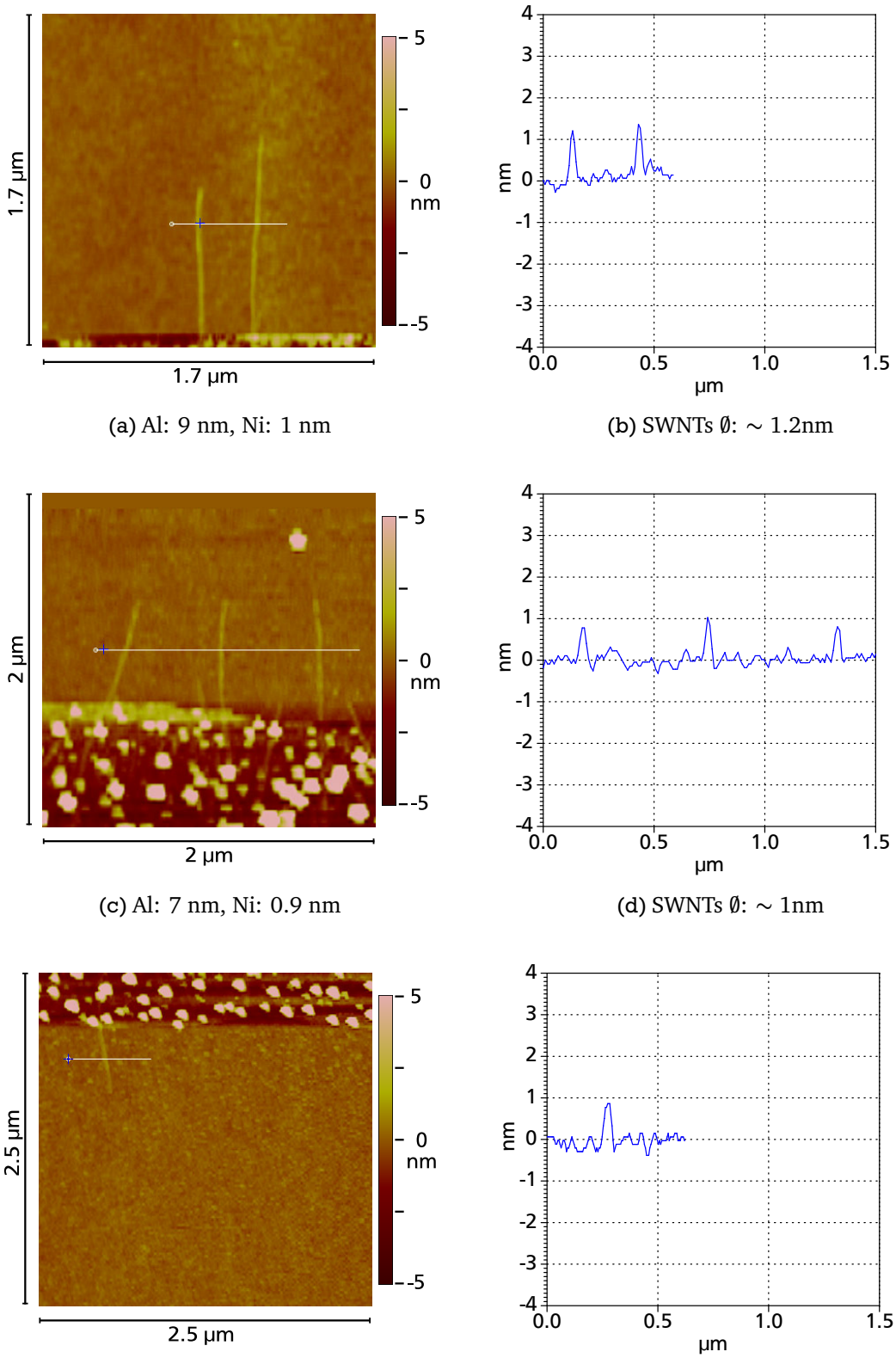

(a) Al: 9 nm, Ni: 1 nm

(b) SWNTs Ø: ∼ 1.2nm

(c) Al: 7 nm, Ni: 0.9 nm

(d) SWNTs Ø: ∼ 1nm

(e) Al: 5 nm, Ni: 0.9 nm

(f) SWNTs Ø: ∼ 1nm

Figure 3.16: Influence of Al thickness on SWNT diameter for a constant Ni nominal thickness (∼ 1 nm). Left column: AFM scans (height). Right column: cross sections along corresponding white lines.

further the Ni layer from 5 to 1 nm, the diameter reduction is no longer present. SWNTs are still dispersed between 1 and 2 nm and some "thick" MWNTs remain on the catalyst area (not to be seen on the AFM scan, as explained in subsection 3.2.4). Obviously, SWNT growth is not only controlled by the Ni thickness alone, but also by the Al underlayer. A 10 nm thick Al layer is too thick to catalyze selectively 1 nm diameter SWNT growth.

To obtain the growth of thinner and more regular SWNTs, the thickness of aluminum is reduced whereas the thickness of Ni remains at 1 nm. Fig. 3.16 compares the diameter of SWNTs grown with 1 nm Ni on 9, 7, and 5 nm. In fact, the aluminum has also been found to influence the diameter of SWNTs, as well as their density. Decreasing the aluminum layer from 10 to 9 nm (see Fig. 3.15 for the combination 1 nm Ni on 10 nm Al), a small decrease in SWNT diameter can be observed (from 1.5 nm to 1.2 nm) and further to 1 nm (for 7 nm Al). Interestingly, even further decreasing aluminum thickness does not affect the SWNT diameter which stays around 1 nm. However, the density of the tubes is found to be drastically reduced (see also Table 3.1). Observing several scans on different places and wafers, it can be statistically confirmed that with 7 nm Al, there is, on average, 1 SWNT each μm^2. With 5 nm Al as underlayer, only 1 SWNT each 25 μm^2 on average covers the wafer. As a conclusion of these two last experiments, the total thickness of the catalyst seems to play a very important role in determining the diameter and spacial density of carbon nanotubes. Concerning the density, these results are in accordance with observations from Seidel et al. [79].

Diameter uniformity of SWNTs is also investigated. Locally, the distribution of CNT diameter

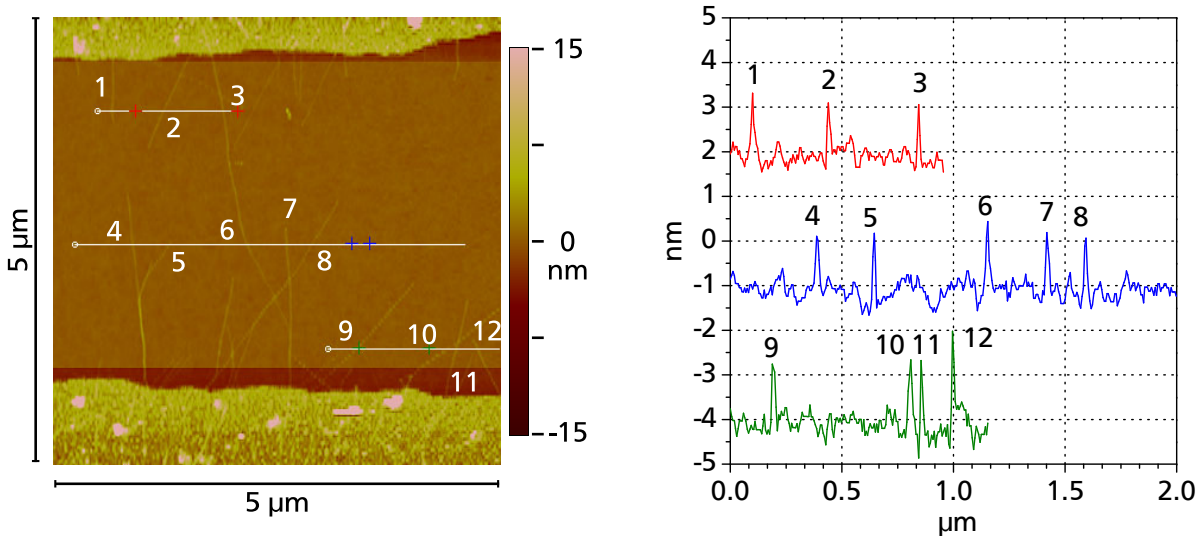

(a) AFM scan (height)

(b) cross sections along the white lines

Figure 3.17: Diameter uniformity of SWNTs grown from the same catalytic structure.

SWNT label	1	2	3	4	5	6	7	8	9	10	11	12
SWNT diameter (nm)	1.4	1.3	1.3	1.3	1.5	1.6	1.2	1.5	1.4	1.6	1.6	1.6

Table 3.2: Diameters of SWNTs shown on Fig. 3.17

is found to be very narrow. Fig. 3.17 shows an example of local diameter distribution of SWNTs grown with a 1 nm Ni/10 nm Al catalyst. Twelve different SWNTs have been measured on a 25 μm^2 scan. As a result, the average diameter is found to be 1.4 nm. It confirms the fact that

SWNTs are slightly too thick (i.e., over 1 nm) when the thickness of Al is 10 nm. On the other hand, the distribution is found to be very narrow (±0.1 nm), which is very satisfactory since it is an important prerequisite to obtain reproducible device properties.

Contact between two SWNTs

The contact between two nanotubes crossing each other has been investigated by AFM. In Fig. 3.18, one can see that the height of the "crossing place" is the sum of the two individual heights of the SWNTs, which shows that the nanotubes are lying one on each other. In this

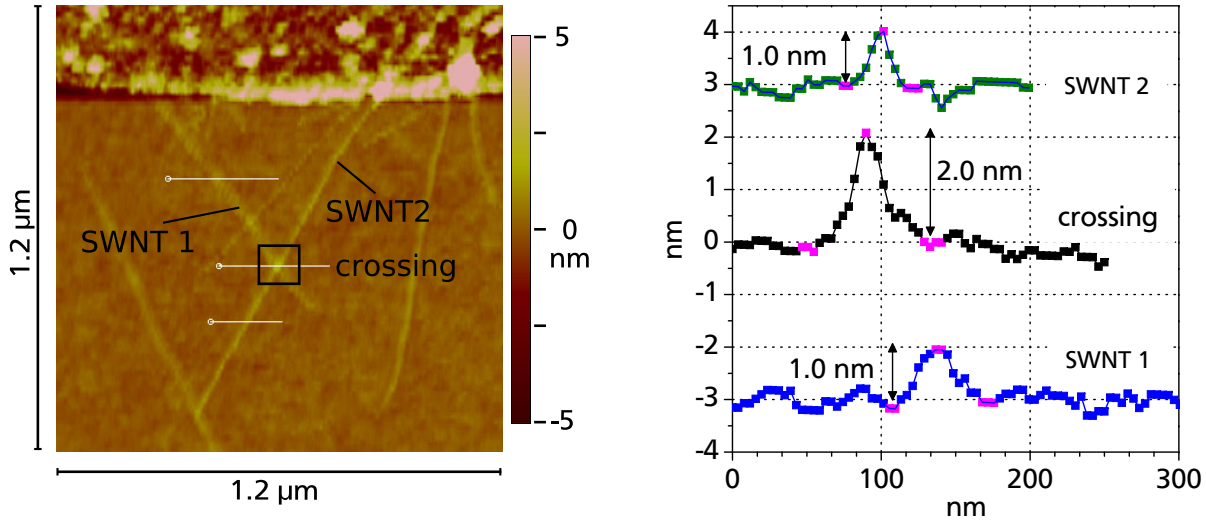

(a) AFM scan (height)

(b) cross sections along the white lines

Figure 3.18: Investigation of SWNT crossing by AFM: the height of the crossing place is exactly the same as the addition of the two SWNTs heights.

case, due to Van der Waals forces, a distance of around 0.34 nm should normally separate them. However, Hertel et al. [85] shows that two nanotubes lying on each other on a substrate are pressed on each other and the Van der Waal distance is reduced due to the substrate attraction.

The electrical contact formed at the crossing place has been analyzed in-depth by Fuhrer et al. [86] at ultra low-temperatures (∼ -220°C to -70°C). They show that the crossover of two m-SWNTs forms a nearly perfect point contact. The tunneling probability is very high and the total conductance is equivalent to the individual conductance of one SWNT. The same result has been found for the junction of two s-SWNTs when they are turned on by field-effect at negative gate voltages. The case of mixed junctions, i.e., metallic to semiconducting SWNTs, is more complicated. Fuhrer et al. demonstrate that not only a tunnel barrier but also a Schottky barrier at the s-SWNT/m-SWNT-contact limits the current. It is then important that the voltage applied to the SWNTs is sufficiently high (above 200 mV) and that the positive voltage is applied to the s-SWNT whereas the negative voltage is applied to the m-SWNT. If not, the resistance is found to be largely increased when compared to the resistance of a single s-SWNT.

These investigations imply two statements for later FET applications reported in this work:

• Since our fabricated FETs are always measured at room temperature with a drain bias of -400 mV, the rare transistors in which a channel is formed at the crossing of a m- and s-SWNT are expected to work similar to the one formed by a single s-SWNT, whereas the source-drain

current may be slightly reduced. Also, the devices could, in this case, show an unsymmetrical behavior, i.e., much more current would flow when the electrode linked to the s-SWNT has a positive voltage and the other electrode, linked to the m-MWNT, is grounded. Interchange of the role of the two electrodes, i.e., source and drain, would drastically reduce the current flow.

• For devices in which the channel is formed by two s-SWNTs crossing each other, the operation of the FETs is expected to be identical as for FETs with a single s-SWNT as channel.

• Only devices with two m-SWNTs crossing each other would behave like a device with a single m-SWNT as the channel, i.e., they would be defective since no change in the conduction would occur under positive or negative gate voltages.

As a conclusion, the probability of obtaining a defective device (i.e., with a purely metallic behavior) decreases from 1/3 to 1/9 for devices with crossed SWNTs as the channel. Moreover, the probability that a device works even if a SWNT alone is not long enough to bridge the source and drain electrodes is increased, since devices with two small SWNTs crossing each other are also suitable.

3.2.4 Limitations of AFM

Several limitations in the utilization of the AFM have to be noted. First, it is impossible to obtain a scan of MWNTs on catalyst because they are standing vertically on the metallic areas (see Fig. 3.9) and the principle of the AFM does not allow the measurement of structures which are not in the plane of the scan. If the AFM tip encounters such a MWNT, then the scan often becomes corrupted and unusable. An example of such an effect is shown in the bottom part of

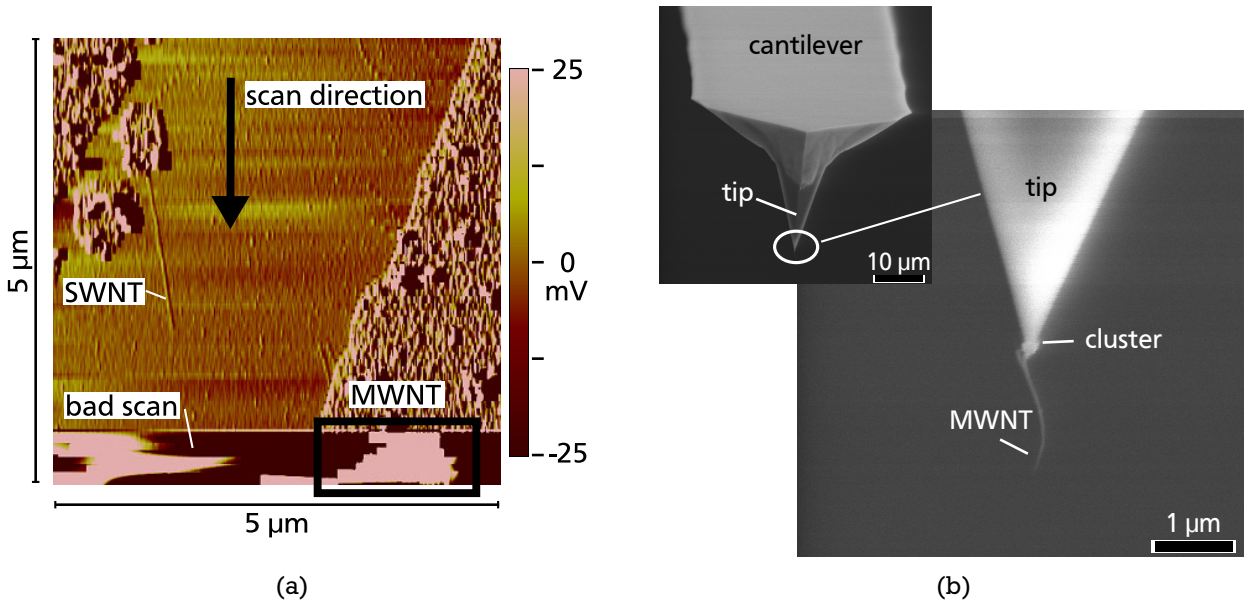

Figure 3.19: (a): Corrupted AFM scan (amplitude) resulting from MWNT adhering to AFM tip. (b): Inset: SEM micrograph of AFM cantilever, magnification x 2000. Enlargement of tip reveals cluster and MWNT which hang on it, magnification x 20,000.

Fig. 3.19a. Even more surprising, Fig. 3.19b shows SEM micrographs of an AFM tip after having measured a catalytic area covered by MWNTs. They reveal that the tip really picks up a cluster with an MWNT hanging on it! Scanning on MWNTs should definitely be avoided.

Another well-known problem of the AFM is the distortion occurring on nanometer size object due to the finite diameter and the non negligible curvature of the tip at the nanoscale. As

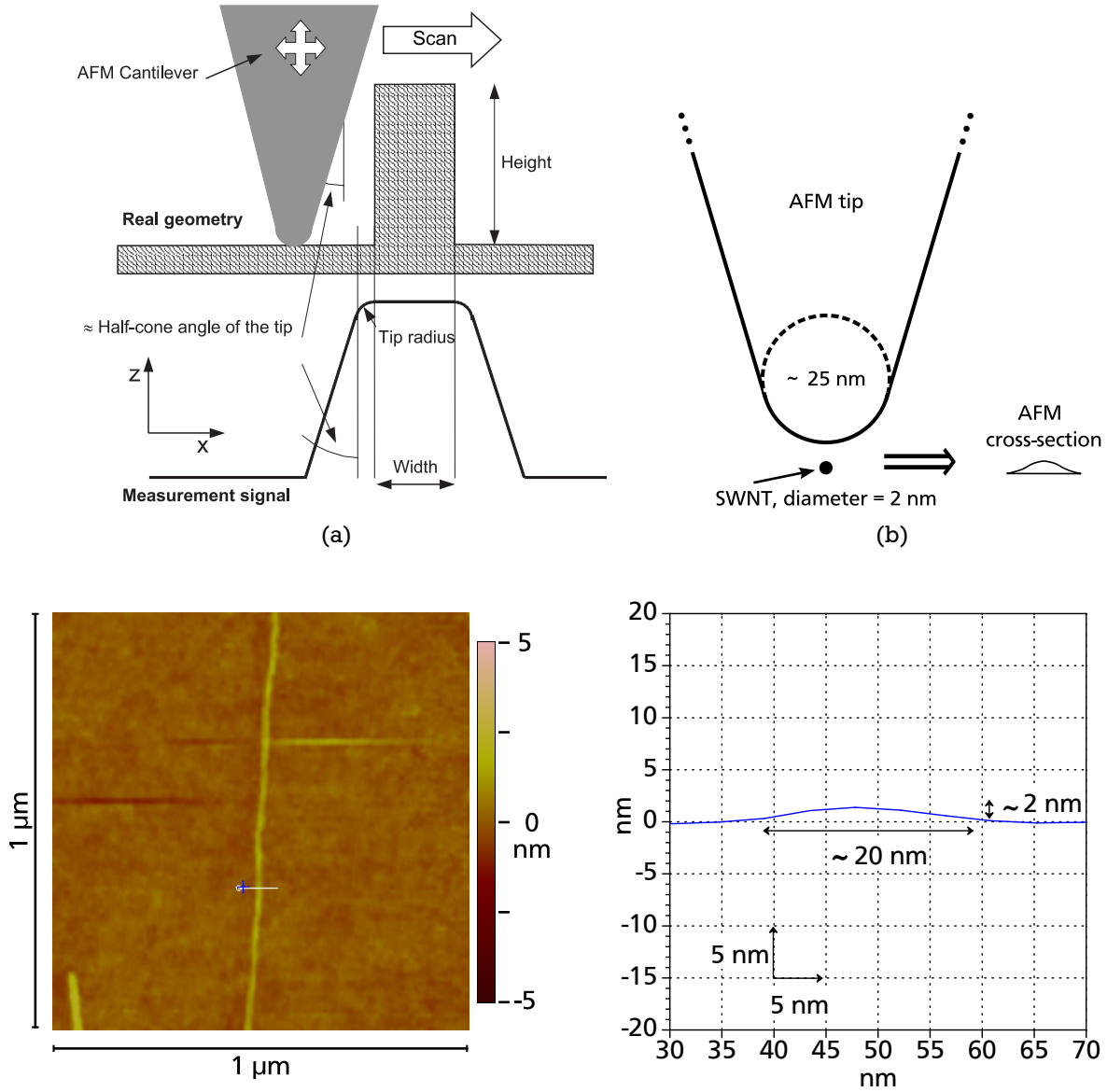

Figure 3.20: (a): Impact of cantilever geometry on AFM scan results [87]. (b): Shape distortion occurring when measuring a CNT by AFM. (c) and (d): AFM measurement of SWNT illustrating the distortion problem.

reported by Hübner et al. [87], the tip shape has a significant influence on the results of the AFM measurement. The minimum sidewall angle of the investigated structure which can be measured is the half-cone angle of the tip used. Additionally, the sharpest edge detectable is limited to the radius of the tip, as illustrated in Fig. 3.20a. When a CNT is scanned, the profile obtained is broadened, as shown in Fig. 3.20d. For the AFM measurements of SWNTs, this means that only the height is reliable for evaluating the diameter since the width always appears misleadingly larger. Fig. 3.20 bottom row shows an example of an AFM scan on a SWNT. The corresponding cross-section shows identical vertical and horizontal scales for illustration purpose, which is usually not the case in the AFM cross sections shown in this work. It can

clearly be seen that the width is ten times larger than the height. All diameter measurements reported in the previous section and in this entire work are only based on the height value read in cross sections.

Finally, the traditional AFM shown in this section has the restriction that it allows the detection and measurement of thin SWNTs (diameters between 1 and 3 nm) only when they are lying on an almost perfectly smooth surface, like e.g. SiO_2 with a surface roughness well below 1 nm. With a surface roughness of several nm, it becomes impossible to measure any nanotube properly (see Fig. 3.7). We demonstrate for the first time the use of the so-called conductive AFM (C-AFM) as a novel solution to this problem. This is explained in the next section.

3.3 Conductive atomic force microscopy (C-AFM) on SWNTs

3.3.1 Principle of C-AFM

The principle of the C-AFM technique is to apply a bias between AFM chuck and tip and measure the current passing through the tip as illustrated in Fig. 3.21. The tip is coated with a conductive material, e.g. platinum-chromium. In the case of a conductive path between the chuck and the tip through the sample, a current is detected by an amplifier electrically connected to the tip. The electrical signal is synchronized with the topographic scan, so that topography and current images are simultaneously obtained within the same scan. However, the C-AFM has to be operated in the contact mode (see section 3.2.1). As a result, the resolution of the C-AFM height measurements is lower than the one of the tapping-mode height scans. In this work, the topographical pictures obtained within a C-AFM scan are called “C-AFM scans (height)”whereas the electrical pictures are called “C-AFM scans (current)”. They are compared to tapping-mode AFM measurements, i.e., “AFM scans (height)” or “AFM scans (amplitude)”.

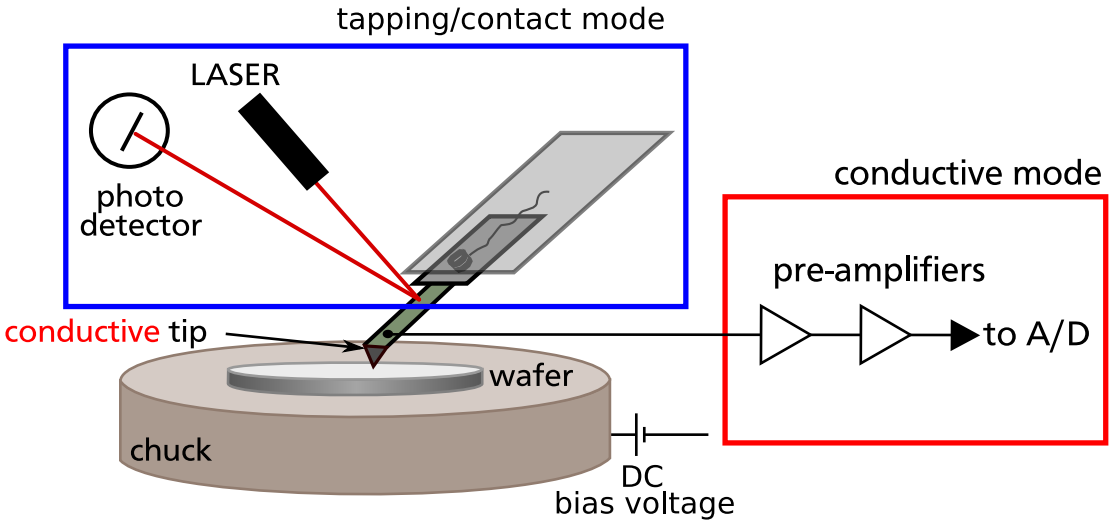

Figure 3.21: Schematic of C-AFM measurement setup.

3.3.2 C-AFM measurements on SWNTs

In order to be able to measure SWNTs electrically with the C-AFM, a current path must be provided from the nanotubes to the silicon substrate. Of course, this would be possible by growing CNTs directly on the Si substrate. However, this would alter the fabrication process. As mentioned in subsection 3.2.2, SiO_2 as catalyst support seems to be a necessary condition to grow nanotubes. Some tests have shown that no CNTs at all can be grown for example on a Ti underlayer. Moreover, if no oxide separates the nanotubes from the substrate, the tip would permanently detect a parasitic current which would reduce the contrast of the current image. To avoid these drawbacks and still maintain the same fabrication sequence, a reduced SiO_2 thickness is used (below 30 nm) which shows leakages at many places on the wafer. Accordingly, if the catalytic areas are sufficiently large, they cover certainly at least one leaky place and a conductive path between the catalyst area and substrate is formed. Simultaneously, the SWNTs which grow from the catalytic areas and fall down on the oxide are still vertically isolated from the Si substrate via the 30 nm thick SiO_2. Only Fowler-Nordheim tunneling current could disturb the measurement. However, 12 V is the maximum bias applicable to the table (in this setup) and the tip has a diameter of $\sim$ 25 nm, which induces an electric field smaller than 4.8 MV/cm. Since no significant Fowler-Nordheim tunneling currents flow through 30 nm thick SiO_2 at electric fields smaller than 6 MV/cm [88], no disturbing background currents exist, which could degrade the image contrast. Only catalytic areas and electrically connected SWNTs are expected to be of the same potential as the Si substrate so that a strong current is detectable when the tip scans SWNTs or catalyst areas.

As a result, very explicit current images of the structures are obtained. Three examples of C-AFM scans (current image) on SWNTs/catalyst are shown in Fig. 3.22. The voltage which must be applied to the chuck to obtain a satisfying scan differs according to the erosion/oxidation of the tip. With brand-new tips, only several tens of mV have to be used to obtain an unambiguous overview. However, when the tip has already been used a couple of weeks for measurement, several volts may be necessary to obtain measurable currents. In the scans in Fig. 3.22, the bright areas represent the catalytic structures (Al/Ni) whereas the dark and uniform color which corresponds to 0 pA, represents the insulating SiO_2 underlayer. The catalyst is found to be conductive, as expected for Al/Ni. The SWNTs and the SWNT connections between the catalytic areas are clearly visible, much better than in the tapping-mode AFM images, where SWNTs are only visible when the underlayer is perfectly smooth. Increased surface roughness of e.g. 2 nm largely degrades the image contrast, so that it becomes impossible to identify SWNTs unambiguously (see Fig. 3.7). This problem is absent in the C-AFM current image, since, regardless of the surface roughness of the underlayer, the current amplitude of the background signal will remain close to zero if the underlayer is isolating, as with SiO_2. SWNTs can be clearly seen in the current image because of the superior signal-to-noise ratio of the C-AFM (current) scan compared to AFM height and amplitude scans.

Fig. 3.22d demonstrates a first attempt of nanoscale resistance measurement of individual SWNTs by C-AFM. In this case, the tip stays at a fixed position in contact with the SWNT and a bias ramp is applied, so that the current-voltage (I-V) characteristic is obtained, from which the total resistance between the tip and the chuck can be calculated. The fairly high value of 70 MΩ probably results in part from the high intrinsic resistance of the SWNT. Here the SWNT is most likely semiconducting and is in the off-state since no appropriate gate bias is applied to turn it

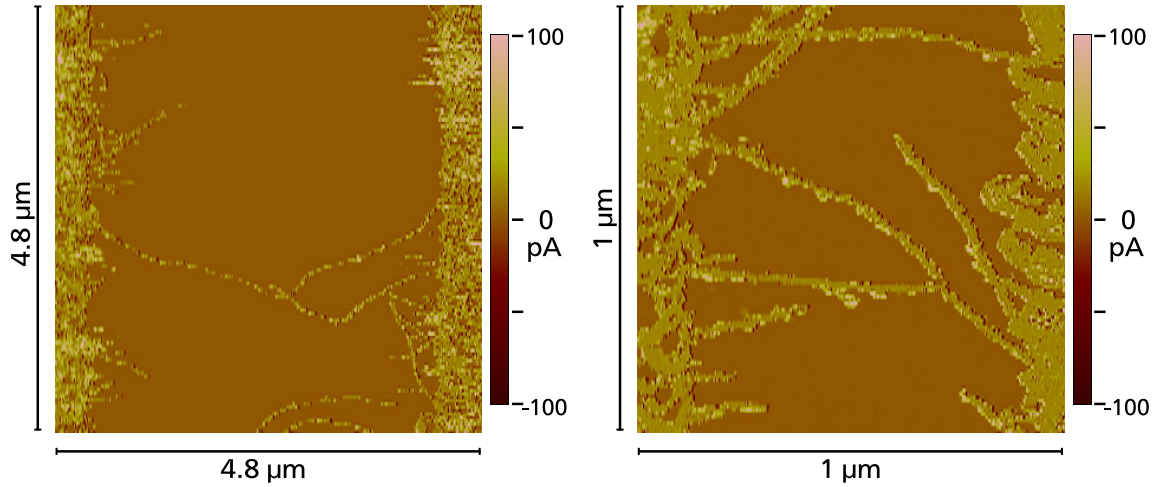

(a) Chuck voltage: -20 mV

(b) Chuck voltage: -20 mV

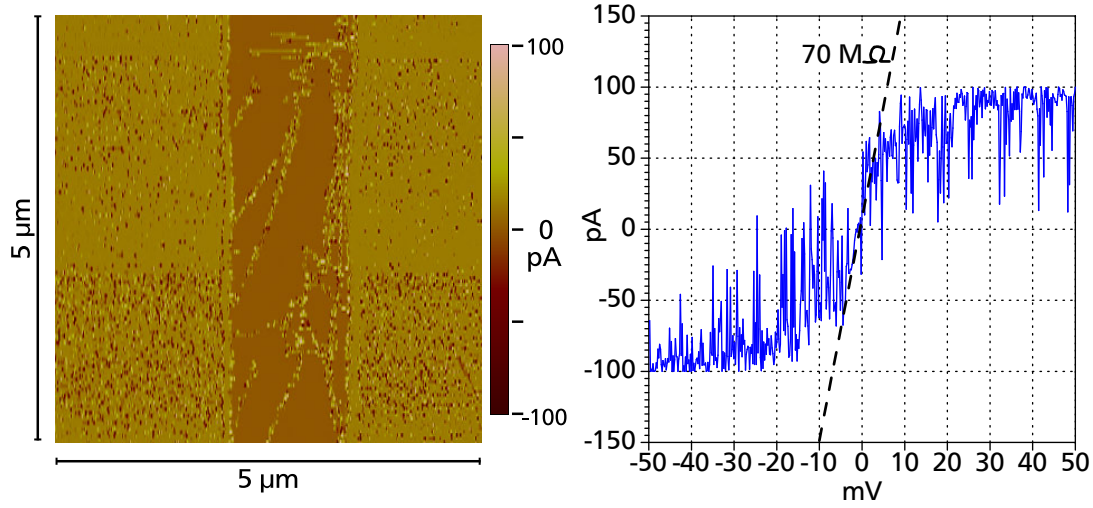

(c) Chuck voltage: +5 V

(d)

Figure 3.22: (a) to (c): C-AFM scans (current) where bright areas show catalytic areas (Al/Ni) and connected CNTs. (d): Example of I/V sweep measured on SWNT.

on. The value of 70 MΩ for s-SWNT resistance is in agreement with the results from Bachtold et al., who obtain a resistance of 60 MΩ on s-SWNTs measured under similar conditions [89]. Additional contributions to the total resistance are due to contact resistances of CNT to tip and CNT to S/D electrodes as well. In fact, a tip coated with platinum on chromium is used here and Pt is known to lead to poor metal-CNT contact despite high work function (see section 2.3) [55, 90]. The contact resistance between the SWNT and S/D area will be reduced in case of Pd. Due to its high work function and other appropriate characteristics, it allows the formation of SWNT-metal contacts almost free of Schottky barriers [30].

Finally, cross sections are also possible on C-AFM current scans. An example is given in Fig. 3.23. Note that the broadening effect reported in 3.2.4 is also to be seen in both C-AFM

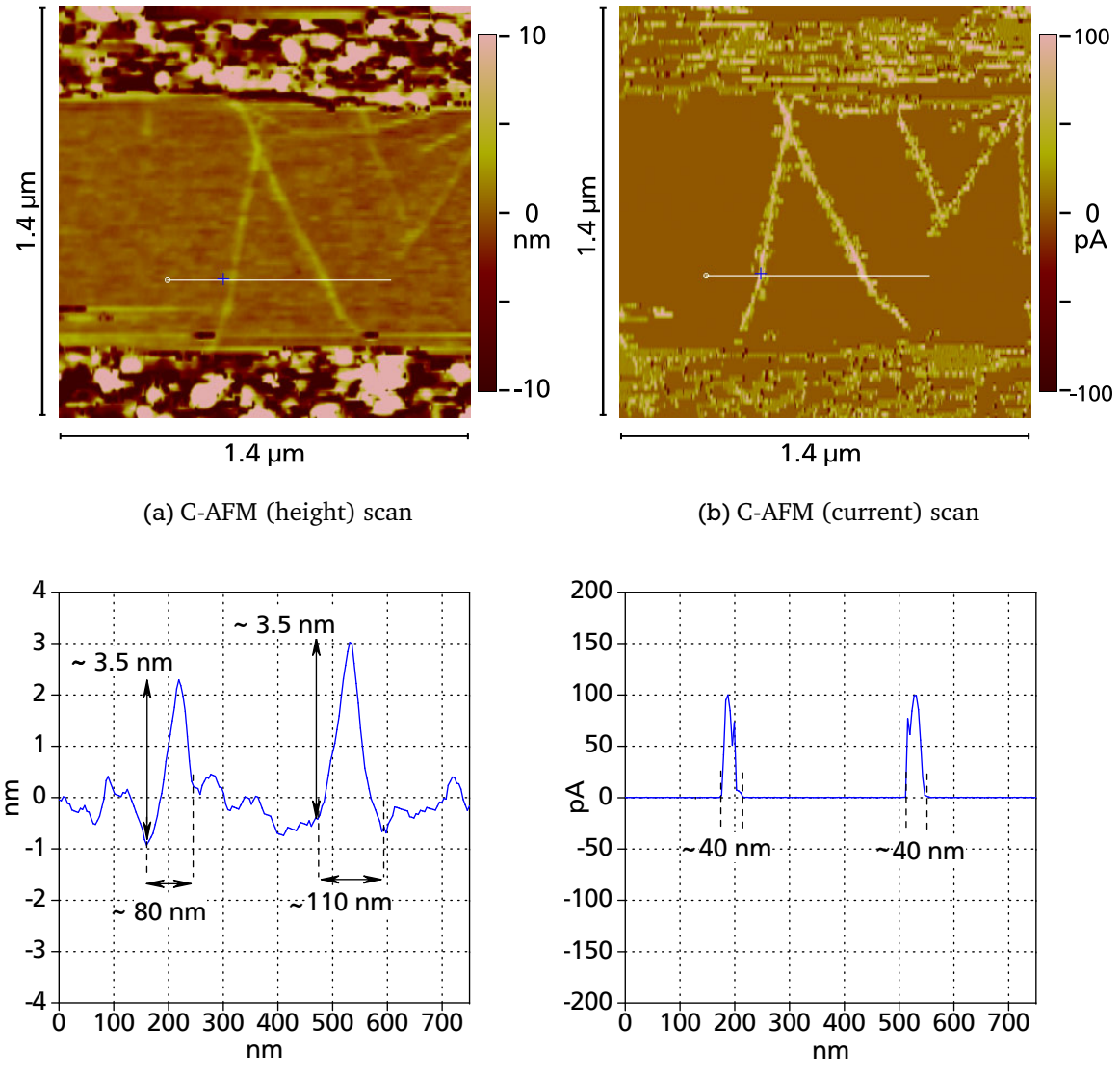

(a) C-AFM (height) scan

(b) C-AFM (current) scan

(c) Height cross section along the white line

(d) Current cross section along the white line

Figure 3.23: Simultaneously measured C-AFM topographical and electrical information illustrating the broadening effect.

height and current images: The widths of the CNTs are broadened in both images. From the cross sections, erroneous widths of 80-110 nm and 40 nm are obtained from height and current C-AFM measurements, respectively. A supplementary boundary noise can be observed at some

places close to the SWNTs on the electrical scan. This may be due to a lateral tunneling current when the tip stands near a SWNT at a very short distance.

3.4 Conclusion

In this chapter, the controlled growth of SWNTs by CCVD on oxidized silicon substrates covered by a catalytic layer composed of nickel on aluminum has been demonstrated. The best parameters found are 1 nm Ni on 5 to 7 nm Al, according to the density which it is intended to be reached. With 7 nm Al, there is at least one SWNT every μm^2. With 5 nm Al as underlayer, only one SWNT every 25 μm^2 in average covers the wafer. The SWNTs have a diameter of 1 ± 0.1 nm.

AFM is found to be a very useful method of measurement for the geometrical and structural characterizations of SWNTs at the nanometer scale. Moreover, AFM provides unambiguous global overviews of structures at the micrometer scale. The major role of the Al underlayer as well as the importance of an oxygen plasma treatment before CVD could be emphasized based on AFM measurements. The catalytic layer thickness could be controlled after electron-beam deposition so that its optimization allowed the control of the SWNT diameter.

Successful C-AFM measurements have been performed on *in situ* connected SWNTs for the first time worldwide (to the best of our knowledge). The SWNTs appear very clearly on the current scan due to the superior signal-to-noise ratio. Measurements of I/V sweeps localized on a point of a SWNT could also be performed.

Based on the study reported in this chapter, the mass-fabrication of field-effect transistors can be started and is reported in the next chapter.